1991A&A...244..257G

Astron. Astrophys. 244, 257–272 (1991)

ASTRONOMY AND ASTROPHYSICS

The nuclear ring of the barred galaxy NGC 4314

J.A. Garcia-Barreto [1,2], D. Downes [1], F. Combes [3,4], M. Gerin [3,4], C. Magri [5], L. Carrasco [2], and I. Cruz-Gonzalez [2]

[1] Institut de Radio Astronomie Millimétrique, Domaine Universitaire, F-38406 St. Martin d'Hères, France
[2] Instituto de Astronomía, Universidad Nacional Autónoma de México, Apdo Postal 70-264, México 04510 D.F. México
[3] DEMIRM, Observatoire de Meudon, F-92195 Meudon, France
[4] Radioastronomie Millimétrique, ENS, 24 Rue Lhomond, F-75231 Paris, France
[5] Physics Department, West Georgia College, Carrollton GA 30118, USA

Received April 30, accepted November 12, 1990

Abstract. We present new observations of the barred spiral galaxy NGC 4314 in the CO(1 – 0) and (2 – 1) lines, the 21 cm H I line, the radio continuum, the visible and the near infrared. The CO observations, made with the IRAM 30 m telescope, show abundant molecular gas in the center of this galaxy, probably in the 12″ circumnuclear ring, in the middle of the strong bar. Even more remarkable is the extreme H I deficiency, as shown by our H I detection with the Arecibo telescope: in NGC 4314, *the $H_2/H\,I$ mass ratio is 60–to–1!*

VLA maps at 2, 6, and 20 cm show several radio continuum sources in a 12″ ring around the optical nucleus. No radio continuum emission was detected from the nucleus itself, the bar or the outer spiral arms. The radio continuum emission has a shallow spectral index of −0.4, and may be a mixture of free-free and synchrotron radiation. Short exposure optical images of the galaxy also show bright spots in a ring around the nucleus, coinciding with the radio continuum structures. Near-infrared photometry of the inner region suggests that the mass-to-2 μm luminosity ratio within a radius of 9″ (450 pc) of the nucleus is 3 $M_\odot/L_\odot$, as in the center of our Galaxy. However, in this region, the H_2 mass is 3 10^8 $M_\odot$, a large fraction of the total mass. Presumably the bar has driven gas into the inner region where it has formed molecular clouds. These clouds produce the O stars ionizing the H II regions seen in the visible and the thermal radio continuum, and supernovae giving rise to the nonthermal radio emission.

Key words: galaxies: barred – galaxies: individual: NGC 4314 – galaxies: evolution of – galaxies: kinematics and dynamics – galaxies: nuclei – radio continuum

1. Introduction

1.1. The hot spot nuclear region

NGC 4314 is an SBa galaxy with a stellar bar 140″ long, and two faint outer spiral arms tracing 130° arcs out to a radius of 125″ from the nucleus. In spite of its very symmetric shape, the galaxy was classed as "peculiar" by Sandage (1961), because of the internal structure in the middle of the bar. This central region has a 2″ × 4″ nucleus, elongated parallel to the bar of the galaxy, two compact, Hα-bright knots (called A and B by Wakamatsu & Nishida 1980) and an S-shaped mini-spiral within an 8″ radius from the nucleus (Sandage 1961; Lynds 1974). In blue light, this mini-spiral starts at the nucleus at p.a. 20°, although it is hard to see from blue images whether the "arms" really are connected to the nucleus. Benedict (1980) claims the central mini-spiral on blue images is an artefact due to a spiral dust pattern; the sites of star formation are in a ring of radius 5″, not a spiral. Indeed, Hα is seen only around the ring, while the "arms" of the mini spiral are starlight, as in the bar (Wakamatsu & Nishida 1980; Lynds et al. 1973). As such, the ring would be a "nuclear ring", in the terminology of Buta (1986). The whole central region is surrounded by a stellar lens or bulge with a radius of 15″ to 20″.

Earlier *UBV* photometry of the nuclear and bar regions showed bluer colors, suggesting star formation, increasing toward the galactic center (Vorontsov-Vel'yaminov et al. 1972; Lynds et al. 1973; Benedict 1980). Indeed, massive stars must have formed in the past 10^7 yr in the nuclear ring, where Hα and [N II] are observed from H II regions (Burbidge & Burbidge 1962; Wakamatsu & Nishida 1980). Interestingly, Hα is quite weak in the nucleus itself: the Hα to [N II] intensity ratio is the standard 3-to-1 in the nuclear-ring H II regions, but only 1-to-3 at the nucleus (Wakamatsu & Nishida 1980). Thus, although NGC 4314 belongs to Morgan's (1958) class of "hot spot nucleus galaxies", there may in fact be *no* hot spots – no emission lines – in the real nucleus of this galaxy. Possibly any residual Hα emission in an aperture centered on the nucleus is contaminated by emission leaking into the aperture from H II regions in the circumnuclear ring, and/or is blended with Hα absorption lines from stellar atmospheres in the central star cluster, which further weaken any residual Hα emission.

The rest of the galaxy is known to be gas poor. Burbidge & Burbidge (1962) noted the bar and the outer spiral arms are devoid of H II regions; van den Bergh (1976) included it in his list of anemic spirals; previous observers didn't detect H I, to a limit of 10^8 $M_\odot$ (Gallagher et al. 1975; Krumm & Salpeter 1976; Huchtmeier 1982).

Send offprint requests to: D. Downes

© European Southern Observatory • Provided by the NASA Astrophysics Data System

1991A&A...244..257G

1.2. Adopted distance to NGC 4314 = 10 Mpc; 1″ = 50 pc

Distance determinations from a Hubble relation are difficult, given NGC 4314's low redshift, and its location on the sky, 15° from the center of the Virgo cluster, requiring corrections for motions of our Galaxy and NGC 4314 toward Virgo. The anomalous H I content may preclude use of a Tully-Fisher relation to estimate distance. The best method is probably to adopt the distance to the galaxy group to which NGC 4314 belongs.

There is general agreement among compilers of galaxy groups that NGC 4314 is a member of a group. It belongs to the Coma I Cloud (Sandage & Tammann 1975) = Group 13 of de Vaucouleurs (1975) = Group 53 of Turner & Gott (1976) = Group 60 of Huchra & Geller (1982) = Group 14-1 of the Coma Sculptor Cloud of Tully (1988). Curiously, all these investigators assign group membership for NGC 4314 based on an erroneous systemic velocity of 880 km s^{-1} from Humason et al. (1956) instead of the more correct value of 980 km s^{-1} (Kelton 1980; Wakamatsu & Nishida 1980). This error of 100 km s^{-1} probably does not affect the group assignment, however.

De Vaucouleurs (1975) regards NGC 4314 as part of a subcondensation within the Coma I cloud, which he calls the N4274 group, containing at least 13 galaxies in a 500 kpc diameter core surrounded by a 1 Mpc diameter halo. De Vaucouleurs (1975) listed the group's distance as 8.1 Mpc. Sandage & Tammann (1975) gave 10.2 Mpc, and de Vaucouleurs (1979) later gave a revised distance of 13.4 Mpc based on six tertiary calibrators (magnitudes of supernovae and superassociations, diameters, luminosity index). Tully (1987, 1988) lists the group's distance as 9.7 Mpc, from a Hubble constant of 75 km s^{-1} Mpc^{-1} and a model of 300 km s^{-1} motion of our Galaxy toward the Virgo cluster. Given this range of estimates, we adopt a distance of 10 Mpc, for which 1″ = 50 pc, and show distance-dependent quantities with a scaling factor $d_{10} = D/10$ Mpc.

1.3. New observations

This paper describes CO observations of NGC 4314 with the IRAM 30 m telescope, H I measurements with the Arecibo telescope, radio continuum maps with the VLA at 20, 6 and 2 cm, and new, short-exposure, optical images as well as near IR (J, H, K, and L') photometry of the nucleus with a 14″ aperture with the 2.12 m telescope in Baja California, Mexico. We also mapped the 2 μm emission from the nuclear region with a 7″ aperture and combined our 2 μm results with the data of Devereux et al. (1987) to see how flux varies with aperture size. We estimate the total mass in the nuclear region and compare it with the H I and H_2 masses. A plausible mass model, adjusted to fit the ring velocity, yields the bar pattern speed that gives an Inner Lindblad Resonance at the radio ring. We also discuss the level of star formation induced by the concentration of molecular gas in the circumnuclear region.

2. CO observations

2.1. CO observing method

The millimeter observations were made in 1988–1990 with the IRAM 30 m telescope at Pico Veleta near Granada, Spain. The half-power beamwidth was 20″.5 at 115 GHz and 12″.5 at 230 GHz, and the beam efficiencies appropriate for sources sizes < 50″ were 0.56 at 115 GHz and 0.45 at 230 GHz; a point source with 1 K main beam brightness temperature has a flux density of 4.4 Jy at 115 GHz and 6.7 Jy at 230 GHz. We used cooled SIS mixers with SSB receiver temperatures of 260 and 280 K at 115 and 230 GHz, and SSB system temperatures outside the atmosphere of 900 and 700 K (T_a^*) at 115 and 230 GHz. The spectrometer was a 512 × 1 MHz filter bank, and we smoothed the spectra to 5 km s^{-1}. We observed the CO(1−0) and (2−1) lines simultaneously, by splitting the filter bank in April 1988, and by using two 512 × 1 MHz filter banks in later sessions.

In 1988, we switched between the galaxy and two symmetric reference positions 3′ away in azimuth. Individual scans had 5 pairs of 30 s on- and off-source integrations. In January 1990, we used the wobbling secondary, which gave very flat baselines. Calibrations on ambient and liquid nitrogen loads were done at the start of each scan. Total integration at each position was 15 to 30 min, yielding 30 mK r.m.s. noise in smoothed spectra. Pointing was checked every 2^h by continuum scans of quasars and planets. The pointing errors were 5″ r.m.s. in daytime and somewhat less at night.

2.2. CO results

In both CO lines, the spectra (Fig. 1) are double-peaked in the center, characteristic of a ring-like structure, with a minimum at the systemic velocity. The strongest CO peak is at 1050 km s^{-1}, in the NW, near a bright part of the circumnuclear ring on the optical image. This CO maximum is especially prominent in maps of line integrated CO emission (Fig. 2). The channel maps in the two CO lines (Fig. 3) show the variation of velocity along the major axis, due to the inclination of the galaxy. The direction of maximum CO velocity gradient is close to that of Hα (p.a. 121°, Wakamatsu & Nishida 1980), and the optical bar (p.a. 145°). The angular resolution is not good enough to show details of the CO structure; the existence of a ring is only hinted at by the double-peaked spectra (Fig. 4a). For comparison, the radio continuum ring has a diameter of 12″, the size of our CO(2−1) beam, and this is likely to be the size of a CO ring as well.

We used a Gaussian smoothing program to convolve the CO(2−1) map to the 20″.5 resolution of the 1−0 map. In the spectra at $(\Delta\alpha, \Delta\delta) = (-6'', +8'')$, (Fig. 4a), the integrated intensity ratio is $I(2-1)/I(1-0) = 0.7$, typical of subthermal excitation of the CO(2−1) line, with slightly different ratios on the blue and red-shifted peaks. We also observed ^{13}CO(2−1) at three positions: at $(\Delta\alpha, \Delta\delta) = (6'', -8'')$ from the nucleus (Fig. 4b), we found $I(^{12}\mathrm{CO})/I(^{13}\mathrm{CO}) = 6$. At (0″, 0″) and (−6″, 8″), the ^{13}CO(2−1) emission is weak, and in the average of the three positions, only the 950 km s^{-1} component shows up clearly (Fig. 4c). This indicates the CO lines are more opaque toward the SE part of the optical ring, which Benedict (1980) claims to be the site of greatest star formation. The NW side of the ring may be hotter and less opaque in ^{13}CO. The ^{12}CO/^{13}CO ratio averaged over the profile is ∼12. The CO(2−1)/(1−0) and ^{12}CO/^{13}CO ratios are both normal, so the standard $M(\mathrm{H_2})/L_{\mathrm{CO}}$ value of 5 $M_\odot$ K km s^{-1} pc^2, is probably a good approximation. With this value, we derive a total H_2 mass of 2.5 10^8 d_{10}^2 $M_\odot$.

2.3. The CO distribution

The CO emission declines strongly along the bar, away from the inner region. There is a factor of ≧10 contrast in CO intensity between the region of the optical ring and the bar outside. Our maps are consistent with all the H_2 being in the circumnuclear ring, with little or no CO emission from either the bar or the

© European Southern Observatory • Provided by the NASA Astrophysics Data System

1991A&A...244..257G

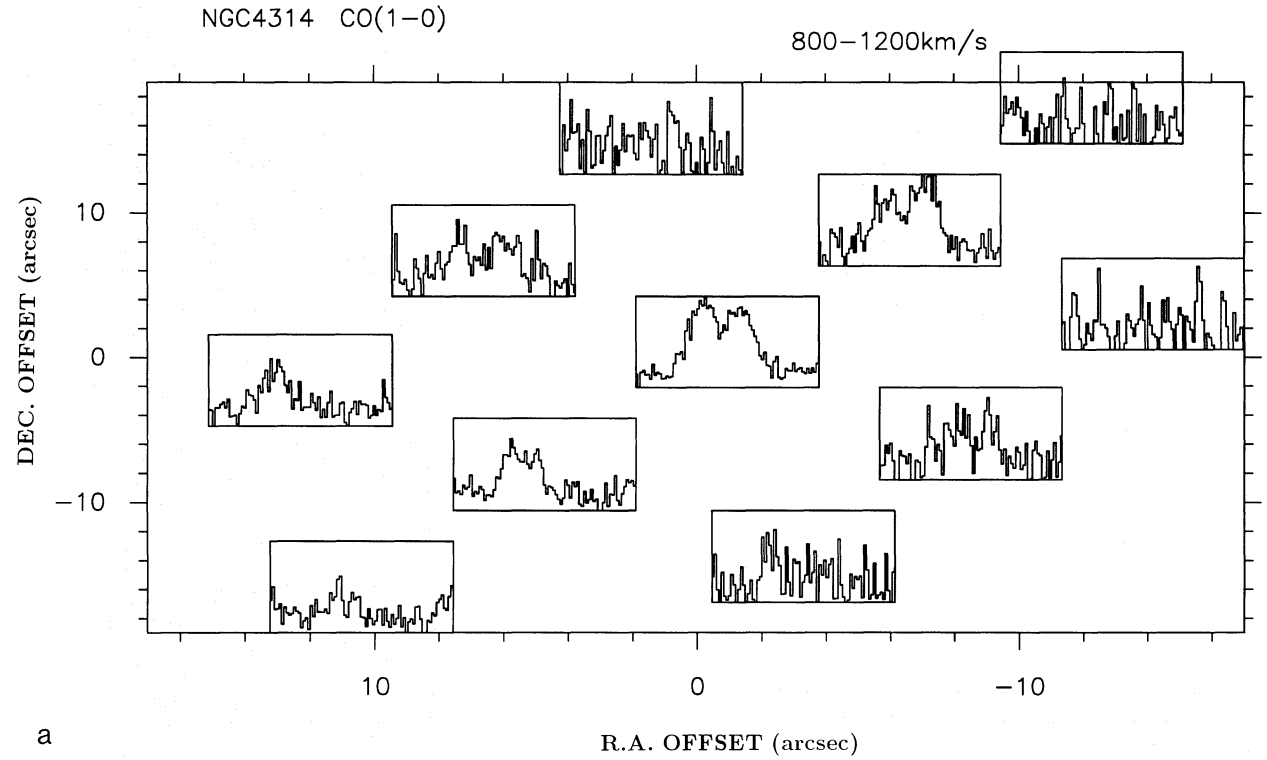

a

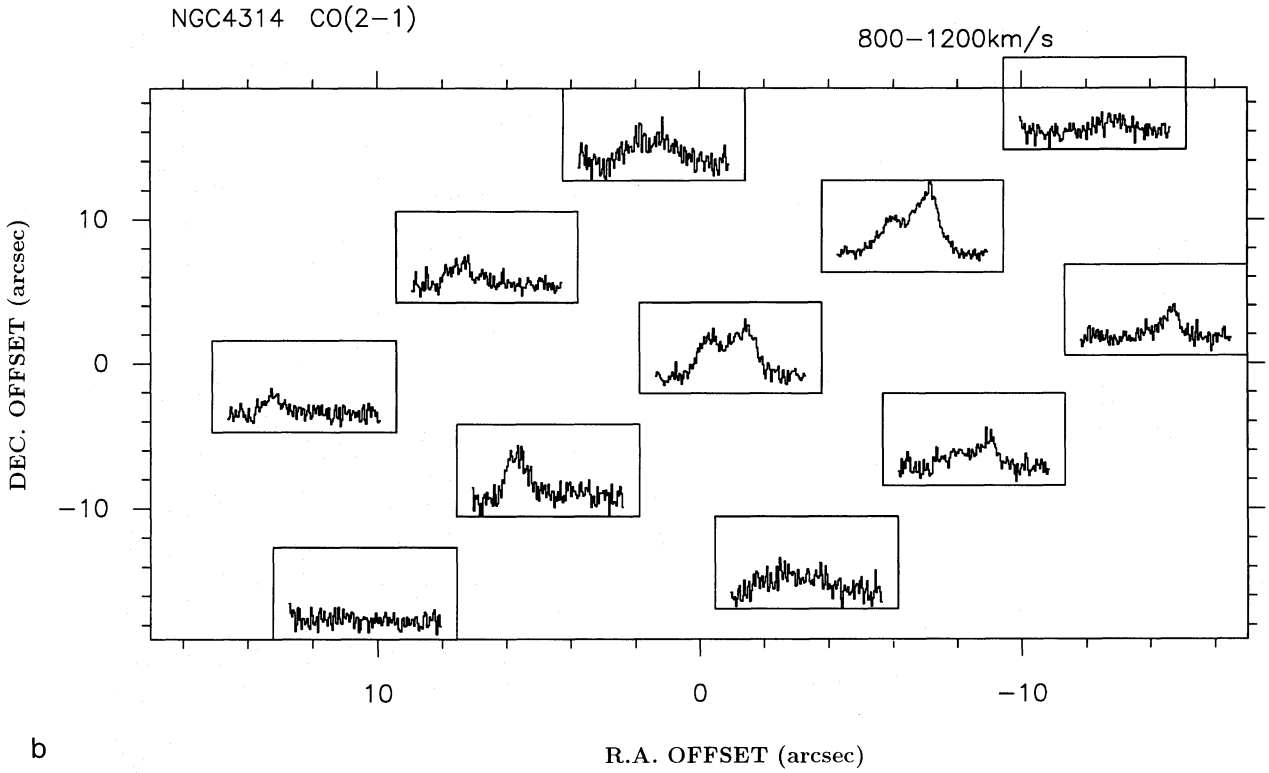

b

Fig. 1. **a** CO(1 − 0) and **b** CO(2 − 1) spectra of NGC 4314, taken with the IRAM 30 m telescope. The velocity resolution is 4.6 km s^{-1} and 2.3 km s^{-1} respectively. The half-power beamwidths are 20″.5 and 12″.5, and the 10″ sampling grid is parallel to the bar. R.A., Dec. offsets are relative to 1950 R.A., Dec. = 12^{h}20^{m}01^{s}.8, 30°10′21″. Scales in spectral boxes: horizontal scale in both CO lines: v_{hel} = 800 to 1200 km s^{-1}; vertical scales: T_{mb} = −0.06 to 0.25 K for CO(1 − 0), T_{mb} = −0.09 to 0.36 K for CO(2 − 1)

© European Southern Observatory • Provided by the NASA Astrophysics Data System

1991A&A...244..257G

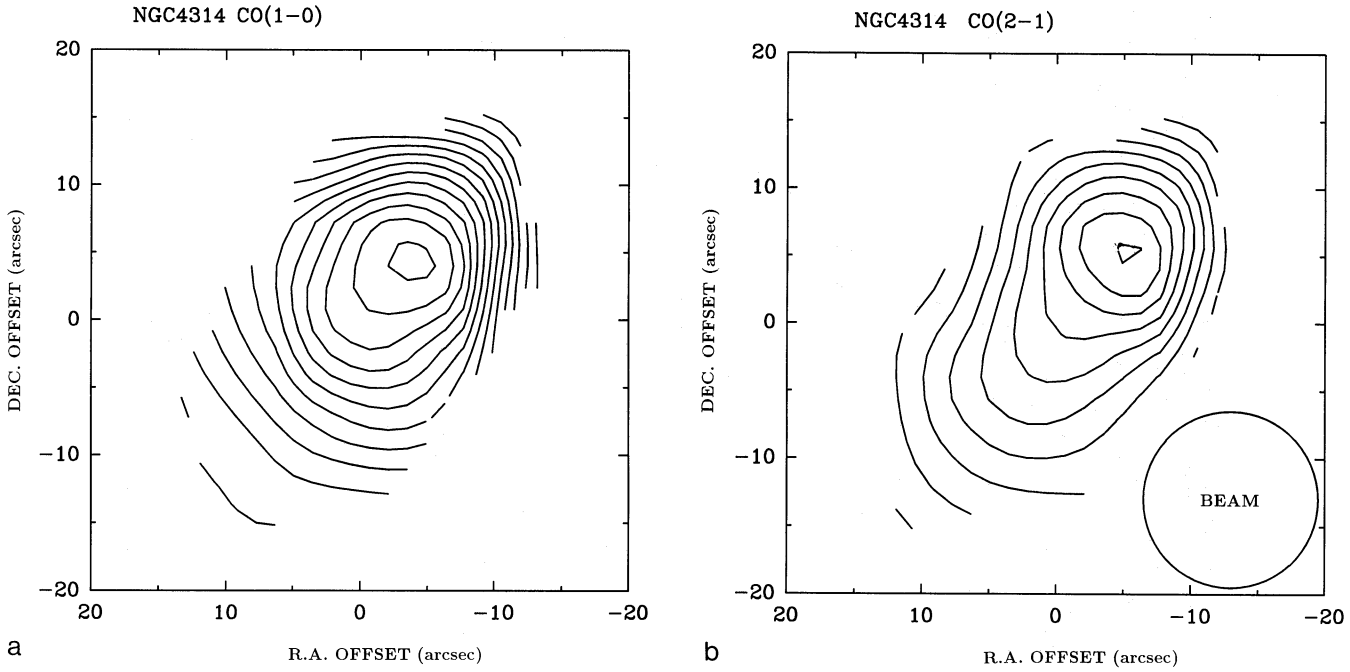

Fig. 2a and b. Contours of line-integrated intensity, $I_{CO} \equiv \int T_{mb}\, dv$ of **a** CO(1 − 0) and **b** CO(2 − 1). The lower right circle in the CO(2 − 1) map is the 12″.5 beam. R.A., Dec. offsets are relative to the same zero position as in Fig. 1. Contours, CO(1 − 0): 2 to 14 in steps of 1, unit = 2.5 K km s^{-1}, peak = 37 K km s^{-1}. CO(2 − 1): 1 to 9 in steps of 1, unit = 3.6 K km s^{-1}, peak = 30 K km s^{-1}

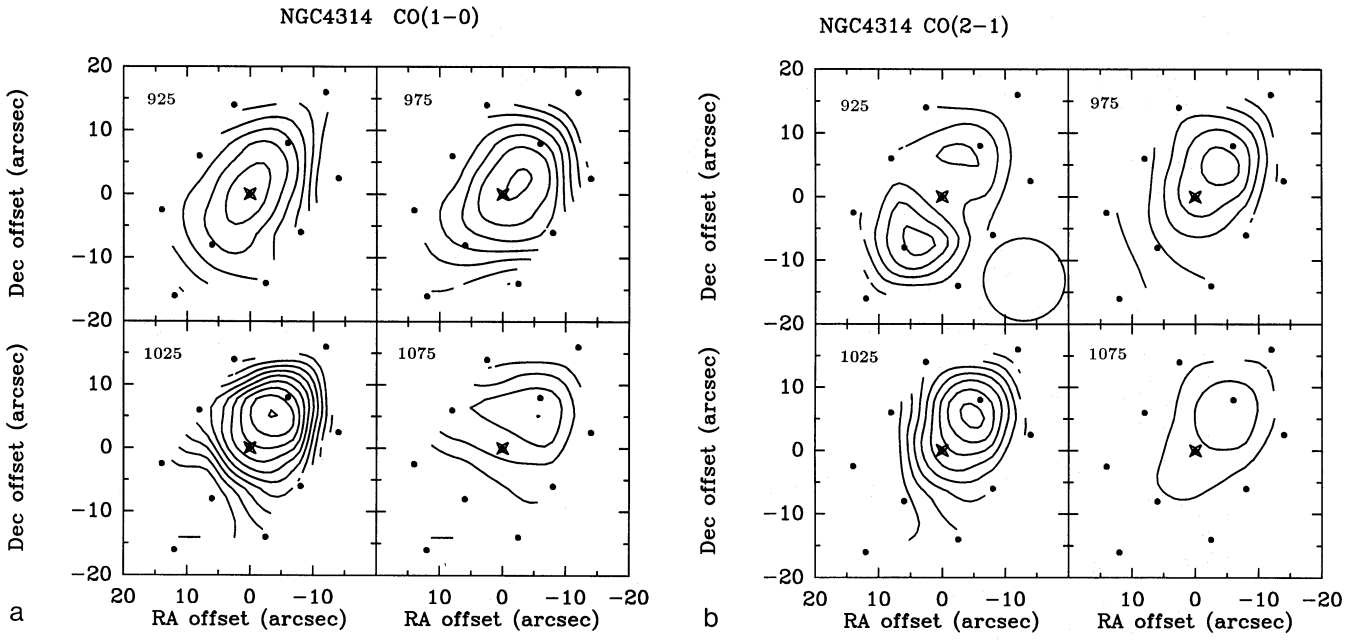

Fig. 3a and b. Channel maps of $I_{v_1}^{v_2} = \int_{v_1}^{v_2} T_{mb}\, dv$ for **a** CO(1 − 0) and **b** CO(2 − 1). Channel width is 50 km s^{-1}, centered on v_{hel} = 925, 975, 1025 and 1075 km s^{-1} (labels in upper left of each box). Contour unit for CO(1 − 0) = 1.23 K km s^{-1}; for CO(2 − 1) = 1.8 K km s^{-1}. Dots = observed points, zero position as in Fig. 1

© European Southern Observatory • Provided by the NASA Astrophysics Data System

1991A&A...244..257G

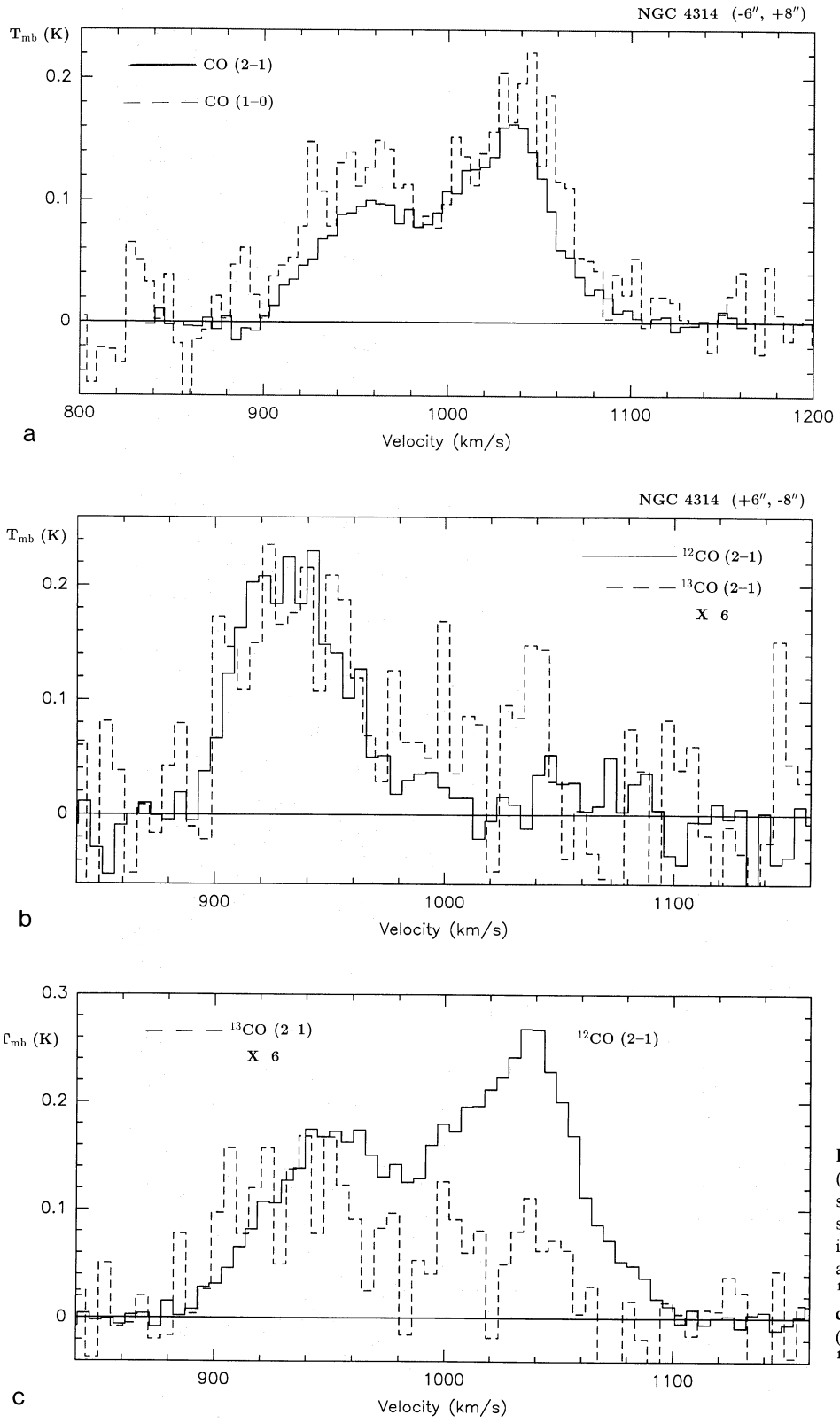

Fig. 4. **a** The CO(1−0) and CO(2−1) spectra at $(\Delta\alpha, \Delta\delta) = (-6'', +8'')$, the position of maximum signal. Both spectra have been convolved to the same angular resolution. The line-integrated intensity ratio is $I(2-1)/I(1-0) = 0.7$. **b** Spectra at $(\Delta\alpha, \Delta\delta) = (+6'', -8'')$ in CO(2−1) and ^{13}CO(2−1) (dashed line; scale multiplied by 6). **c** Averages of spectra at $(\Delta\alpha, \Delta\delta) = (0'', 0'')$, $(+6'', -8'')$ and $(-6'', +8'')$ in CO(2−1) and ^{13}CO(2−1) (dashed line; scale multiplied by 6)

© European Southern Observatory • Provided by the NASA Astrophysics Data System

1991A&A...244..257G

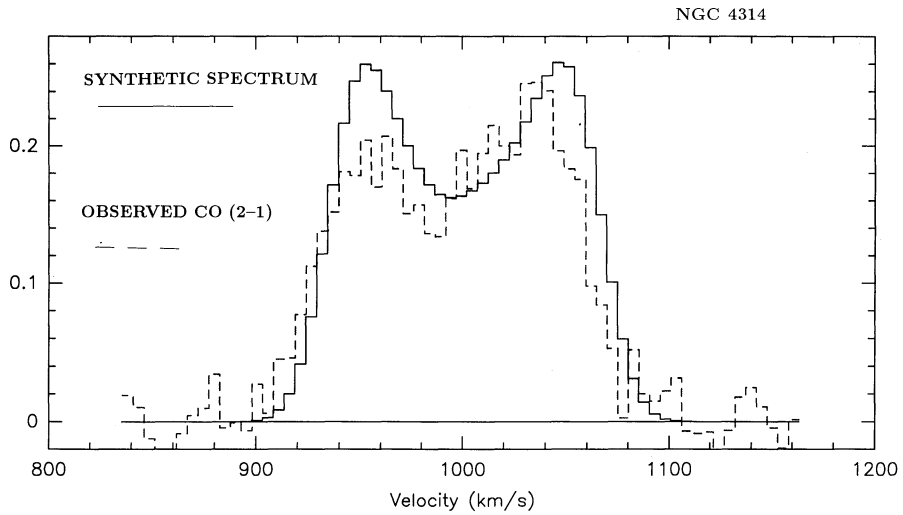

Fig. 5. *Solid line:* synthetic CO spectrum of molecular clouds in a 12″ ring with rotational velocity of 186 km s^{-1} and an inclination of the plane of the sky of 30°, as would be observed with a 12″.5 beam centered on the middle of the ring. *Dashed line:* Observed CO(2−1) spectrum, taken at $(\Delta\alpha, \Delta\delta) = (0'', 0'')$.

interior of the ring. We computed the central CO(2−1) spectrum expected from molecular clouds in a 12″ ring, inclined on the plane of the sky by 30° (Wakamatsu & Nishida 1980), with velocities adjusted to match the observed line profile. The synthetic spectrum is similar to the observed one (Fig. 5), so no CO emission from the nucleus is needed to explain the data.

3. H I observations

3.1. H I *observing method*

The H I observations of NGC 4314 were made in 1987 and 1988 with the Arecibo 305 m telescope and the 21 cm dual-circular polarization feed. Each polarization went to a separate, cooled FET amplifier receiver with a system temperature of 40 K. The tracking feed had a 45 MHz bandwidth, centered at 1418 and 1414 MHz in 1987, and at 1404 MHz in 1988 (the H I line from NGC 4314 is redshifted to 1416 MHz). The half-power beamwidth was 3′.3 and 1 Jy beam^{-1} gives 7.5 K T_a, or 15.5 K T_{mb}. The pointing accuracy was 20″. The signal in each of the two polarizations was split and led to a 2048-channel autocorrelation spectrometer, which gave four 512-channel spectra – two in each polarization – each covering 20 MHz (4000 km s^{-1}), centered on the H I frequency of NGC 4314, with a velocity resolution of 8.3 km s^{-1}. Fluxes were calibrated with continuum sources from the list of Bridle et al. (1972). In 1987, the beam was centered on the optical nucleus of NGC 4314. In 1988, we centered the beam on the nucleus and also 1′.8 NE of the nucleus to check for H I at larger radii.

3.2. *The* H I *deficiency in NGC 4314*

From the line parameters (Table 1), we derive an H I mass of $4\ 10^6\ d_{10}^2\ M_\odot$, a surprisingly low value. Furthermore, the spectra (Fig. 6), show that NGC 4314 is not a normal spiral with a central hole, but is truly poor in H I: the flux at the offset position is consistent with the H I being in the center of the galaxy only, in a source of diameter $\leqq 1'$ ($3\,d_{10}$ kpc). Thus the galaxy's *total* H I mass is extremely low: a typical Sa or SBa galaxy with the angular diameter of NGC 4314 would have a total H I flux nearly three times that measured at its center with the Arecibo dual-circular feed (Haynes & Giovanelli 1984). Relative to the mean H I surface density of spatially isolated SBa galaxies, NGC 4314 is deficient in H I by a factor of 200. Similar H I-poor spirals are usually found in the cores of rich clusters like Virgo and Coma (Haynes et al. 1984), whereas NGC 4314 appears to be in a relatively benign environment. In fact, we know of no other spiral galaxy which is as H I deficient as this one.

By contrast, the H_2 content is normal: for NGC 4314, $M(H_2)/L_{FIR} = 0.3\ M_\odot/L_\odot$, close to the mean value of $0.14\ M_\odot/L_\odot$ for all galaxies, regardless of type (Rengarajan & Verma 1986; Solomon & Sage 1988). However, the H I content is surprisingly low: $M(H_2)/M(H\,I) \geqq 60$! This ratio is well outside the mean values for all morphological classes (Young & Knesek 1989), and even more extreme than the values of 10 to 30 inferred for NGC 4419 (Kenney et al. 1990), and a few other Virgo cluster S0 – Sa galaxies (Kenney & Young 1989). We consider this ratio tobe a lower limit, since the Arecibo beam area is 100 times the CO(1−0) beam area, and we mapped CO only in the central region of the galaxy.

4. Radio continuum observations

4.1. *Radio continuum observing method*

The observations were made with the VLA-D array at 6 and 20 cm in 1984, the B array at 20 cm in 1985, the C array at 6 cm in 1985 and C/D configuration at 2 cm in 1987. Phases were calibrated on the source 1225+368 in the D array, and 1219+285 in the B, C, and C/D configurations. The instrumental polarization at 20 and 6 cm and the flux scales were determined relative to 3C 286. The data were reduced with standard VLA programs (Thompson et al. 1980) for linearly polarized and total intensities. We used two 50 MHz channels, which were calibrated independently and then combined and processed with the modified CLEAN algorithm (Clark 1980). The B, C, and C/D configurations gave similar resolutions at 20, 6, and 2 cm, respectively, and the D array alone provided broader-beam maps at 20 and 6 cm.

4.2. *The radio continuum Maps of NGC 4314*

We made a low-resolution, D-array 20 cm map (not shown here) with a restoring beam of 35″, and detected radio emission only from the central region of the galaxy, and an unrelated 0.8 mJy

© European Southern Observatory • Provided by the NASA Astrophysics Data System

1991A&A...244..257G

Table 1. Line measurements of NGC 4314

Spectral line		H I	CO(1−0)	CO(2−1)
Instrumental				
Rest frequency	GHz	1.4204	115.271	230.538
Half-power beamwidth	arcsec	200	20.5	12.5
Spectral resolution	$km\,s^{-1}$	8.3	5	5
R.m.s. noise	mK	2.3	22	24
Radial velocities at center position				
Heliocentric velocity	$km\,s^{-1}$	982	985	980
Half-power linewidth	$km\,s^{-1}$	160	160	136
Line intensities[a]				
Peak line flux density, S	Jy	0.0011	1.1	2.3
Peak line temperature, T_{mb}	K	0.018	0.26	0.34
Peak intensity, $I \equiv \int T_{mb}\,dv$	$K\,km\,s^{-1}$	3.0	31	30
From maps convolved to 24″	$K\,km\,s^{-1}$	–	23	16
Distance-dependent quantities				
All scale as $(D/10\,Mpc)^2$:				
Line luminosity[b], $L \equiv D_{pc}^2 \int I\,d\Omega_r$	$K\,km\,s^{-1}\,pc^2$	$3\ 10^8$	$5\ 10^7$	$3\ 10^7$
H_2 mass $= 5\,L_{CO(1-0)}$	$M_\odot$	–	$2.5\ 10^8$	–
H I mass[c] $= 2.4\ 10^5\,D_{Mpc}^2 \int S_{Sy}\,dv$	$M_\odot$	$4\ 10^6$	–	–

[a] Peak CO intensity is at $(\Delta\alpha, \Delta\delta) = (-6'', +8'')$
[b] $d\Omega_r \Rightarrow$ integrate over response pattern (beam * source)
[c] H I mass formula from Haynes & Giovanelli (1984)

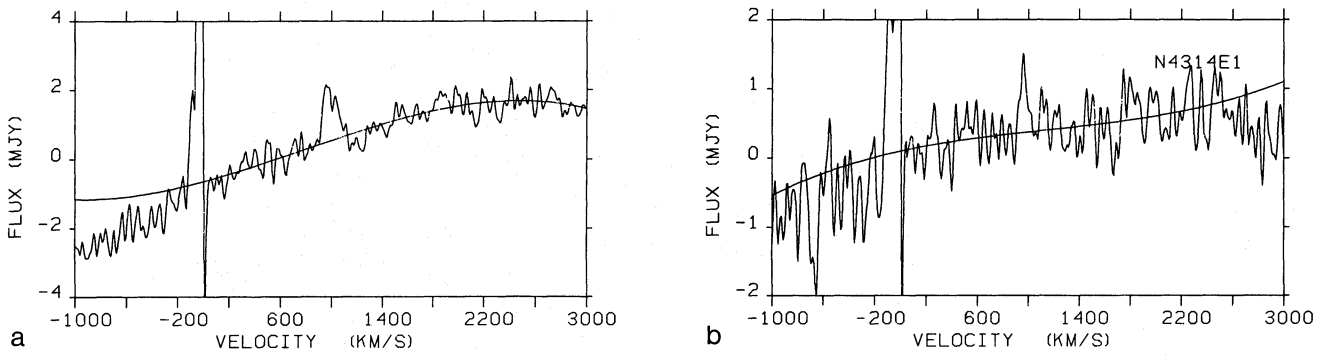

Fig. 6a and b. H I spectra taken at Arecibo. The line from NGC 4314 is at 982 $km\,s^{-1}$; the strong emission near 0 $km\,s^{-1}$ is from our Galaxy. **a** Center position: 1950 R.A., Dec. = $12^h20^m02^s.0$, 30°10′25″. **b** NE offset position: $12^h20^m07^s.8$, 30°11′41″

background point source at $12^h20^m06^s.1$, +30°10′37″ (1950), nearly 1′ NE of NGC 4314's nucleus. There is no emission > 1 mJy (10% of the 20 cm peak) from the bar or the outer spiral arms. We also made a 6 cm total intensity map at low resolution. Peak flux densities from the central region of the galaxy were 10.7 mJy at 20 cm and 2.4 mJy at 6 cm.

Because other 20 cm maps of this galaxy with 38″ resolution (Hummel 1980; Gioia & Fabbiano 1987) did not resolve the central region, we also observed with the B array at 20 cm, the C array at 6 cm and the C/D array at 2 cm, which gave maps with 3″.5 beams. Figure 7 shows the high resolution maps at 20 cm, 6 cm, and 2 cm, and Table 2 gives the flux densities. No polarized emission was detected to a limit of 15% of the peak intensity at 6 and 20 cm.

The radio continuum emission at the three wavelengths comes from an incomplete ring around the nucleus, with inner and outer radii of 4″ and 9″, broken in the southwest. There is no distinct radio peak at the galactic nucleus, to a limit of 0.1 mJy at 20 cm. Any central radio source, if it exists, must be much weaker than the sources in the surrounding ring. This galaxy thus differs from the barred spiral NGC 1097 and the spiral NGC 3310, both investigated with comparable linear resolution at the VLA, in which a compact nucleus is the strongest radio source (Hummel et al. 1984, 1987; Duric et al. 1986).

4.3. Separation of thermal and non-thermal radio emission

At the extremes of our error bars, the radio continuum spectrum can fit a power law of spectral index −0.4, typical of supernova remnants. However, the number of H II regions seen in Hα, the Hα surface brightness, and the fact that the radio spectrum at 2 to 6 cm is flatter than at 6 to 20 cm (Fig. 8), all suggest a mix of

© European Southern Observatory • Provided by the NASA Astrophysics Data System

1991A&A...244..257G

Table 2. Radio continuum measurements of NGC 4314

Frequency (GHz)		1.4649	4.8851	14.9649
Instrumental (clean beam)				
Major × minor axes	(arcsec)	3.5 × 3.5	3.5 × 3.3	4.6 × 2.5
Bandwidth	(MHz)	50	50	50
Integration time	(min)	68	90	285
R.m.s. noise	(mJy)	0.07	0.06	0.1
Flux densities				
Peak flux [a]	(mJy/beam)	0.82	0.47	0.50
Polarized flux	(mJy/beam)	< 0.1	< 0.06	–
Integrated flux	(mJy)	11 ± 1	5 ± 1	3 ± 1
Estimated total thermal flux	(mJy)	2.8	2.7	2.6

[a] From an unresolved source on the radio ring

thermal and non-thermal radiation. We derived the optically thin thermal ($S_t \propto \nu^{-0.1}$) and non-thermal ($S_{nt} \propto \nu^{\alpha}$) fractions of the observed fluxes at 20 and 2 cm, by assuming $\alpha = -0.8$. The result is that 85% of the flux density at 2 cm is thermal, and <25% at 20 cm.

From the thermal flux at 2 cm, and for an electron temperature of 10^4 K, and the <2″ width of the five strongest radio peaks, the electron density is (Mezger & Henderson 1967):

$$\frac{n_e}{\mathrm{cm}^{-3}} = 8.02\ 10^3 \left[\frac{T_e}{10^4\,\mathrm{K}}\right]^{0.175} \left[\frac{\nu}{\mathrm{GHz}}\right]^{0.05} \left[\frac{S_\nu}{\mathrm{mJy}}\right]^{0.5} \cdot \left[\frac{D}{\mathrm{kpc}}\right]^{-0.5} \left[\frac{\theta_G}{\mathrm{arc\,sec}}\right]^{-1.5}, \quad (1)$$

which gives an electron density $>25\,\mathrm{cm}^{-3}$, an emission measure $>5\ 10^4\,\mathrm{pc\,cm}^{-6}$, and an ionized mass $<3\ 10^6\ M_\odot$ for the sum of the five main radio peaks. The corresponding number of Lyman continuum photons is $2\ 10^{51}\,\mathrm{s}^{-1}$, equivalent to the flux from several hundred O7 or earlier type stars. Among galaxies studied with the same resolution at the VLA, NGC 3310 has H II regions with similar electron densities (Duric 1986). The galaxy M83 (Ondrechen 1985) has radio sources of comparable size and surface brightness; part of their flux is also thermal.

From the thermal radio flux, the expected Hα flux, F, is (Lequeux 1980):

$$\frac{F(\mathrm{H}\alpha)}{\mathrm{erg\,cm}^{-2}\,\mathrm{s}^{-1}} = 8.75\ 10^{-10} \left[\frac{S_\nu}{\mathrm{Jy}}\right] \left[\frac{\nu}{\mathrm{GHz}}\right]^{0.1} \left[\frac{T_e}{10^4\,\mathrm{K}}\right]^{-0.34}. \quad (2)$$

For $S_t = 0.3$ mJy at 6 cm, we obtain $F(\mathrm{H}\alpha) \simeq 3.1\ 10^{-13}$ erg cm^{-2} s^{-1} for an individual region, and for the sum of the five main radio peaks on the 6 cm map, the expected Hα flux is $F(\mathrm{H}\alpha) \simeq 1.5\ 10^{-12}$. The observed Hα flux is $4\ 10^{-13}$ erg cm^{-2} s^{-1} (Wakamatsu & Nishida 1980), which would be consistent with the thermal radio flux if the extinction were $A_{\mathrm{H}\alpha} \simeq 1.4$ mag, or $A_v = 1$ mag.

5. Optical observations

5.1. Optical observing method

The optical observations were carried out in 1987 with the 2.12 m telescope of the Observatorio Astronomico Nacional in San Pedro Mártir, Baja California, México, with 1″ seeing. Exposures of 7, 12, and 70 min were taken on Kodak 103 Oa (blue-sensitive) emulsion on glass plates with no filters. Figure 9 shows the 12 and 70 min exposure images. For comparison with the radio maps, we digitized the optical plates on a PDS micro densitometer at the Centro de Investigacion Cientifica y Estudios Superiores de Ensenada, Mexico. The pixel size of 50 μm corresponds to 0″.65. Relative intensities were read at several position angles.

5.2. Comparison of optical and radio images

The 70-min optical exposure (Fig. 9a) shows a tight spiral, within a 10″ radius of the optical nucleus (see also Sandage 1961; Lynds et al. 1973; Lynds 1974; Wray 1988). The "arms" of this mini-spiral are undoubtedly starlight, as they are not seen on the Hα+[N II] image by Pogge (1989). The 12-min exposure (Fig. 9b) shows more clearly the optical continuum from the stars at the nucleus, and also the light from the H II region "hot spots" which are arranged in a ring. If one suppresses the light from the nucleus in Fig. 9b, the resulting distribution of bright spots closely resembles the ring in Hα+[N II] (Pogge 1989) and the radio continuum ring, especially at 6 and 20 cm (Fig. 7).

To verify the coincidence of the features on the optical and radio continuum "rings", we used SAO stars on both our plates and the Palomar Survey to align the short exposure optical image with the 20 cm radio contours, to 1″ accuracy (Fig. 10). We also measured distances from the nucleus to the radio and optical peaks independently. For the optical images, we measured distances between the nucleus and the NW and SE bright spots. For the radio emission, we assumed the nucleus was at the central radio minimum, to an accuracy of 1″.5. Figure 11 shows the relative intensity across the digitized optical image at p.a. 305° (or −55°) compared with the radio continuum; the optical and radio structures coincide. There is no radio continuum peak at the optical nucleus, just as there is no optical line emission there (Pogge 1989).

6. Near-infrared observations

6.1. Near-IR observing method

The near-IR observations were also made with the 2.12 m telescope in San Pedro Martir, Baja California, México, in 1986. We used a single element InSb detector at J (1.2 μm), H (1.65 μm),

© European Southern Observatory • Provided by the NASA Astrophysics Data System

1991A&A...244..257G

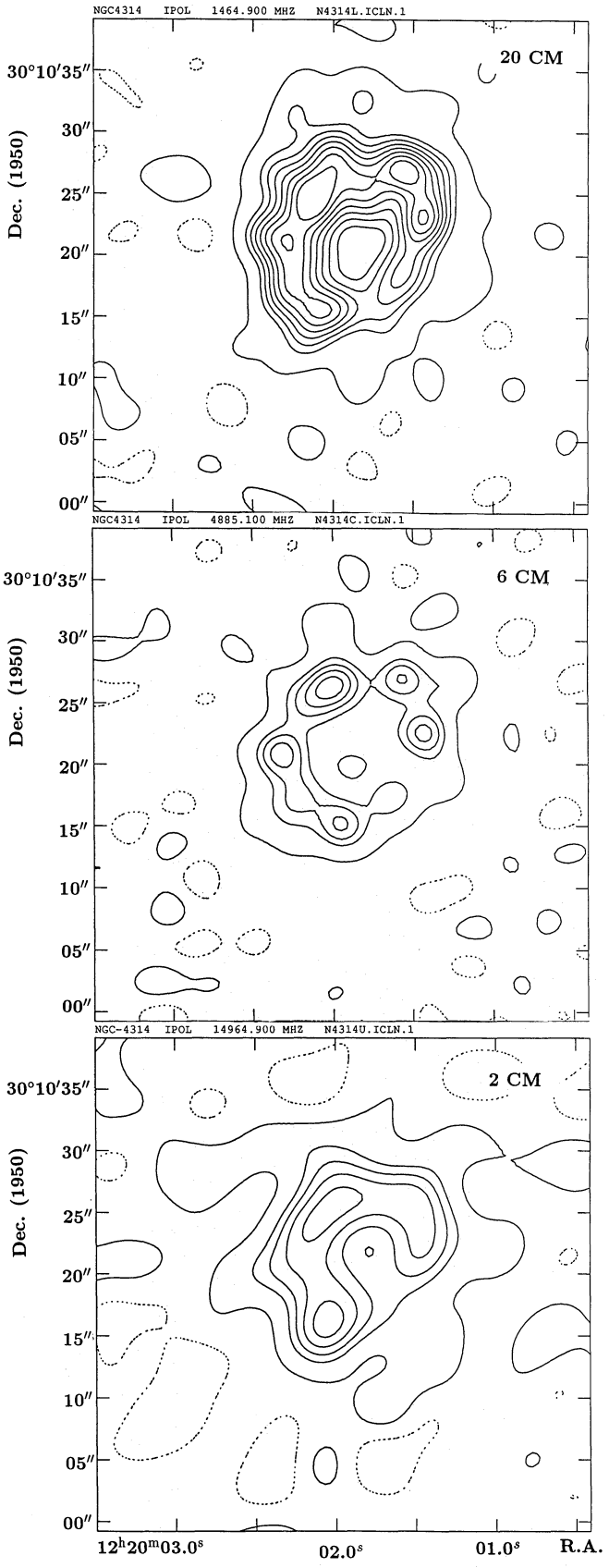

Fig. 7. High resolution maps of radio continuum emission at 20 cm (top), 6 cm (middle), and 2 cm (bottom). On all three maps, contours are $-1, 1, 3, 4, 5, 6, 7, 9$ in units of 0.077 mJy beam area^{-1}

Table 3. Near-infrared photometry of NGC 4314

Filter band	Wavelength (μm)	Flux density (mJy)	
		5″.5 aperture[a]	14″ aperture
J	1.2	32	98±8
H	1.65	42	114±8
K	2.2	32	92±8
L'	3.8	–	37±8

[a] Fluxes in 5″.5 aperture from Devereux et al. (1987)

K (2.2 μm), and L' (3.8 μm) bands at the f/31 Cassegrain focus (Roth et al. 1984). The beam size was 14″, and the 10 Hz chopper throw was 100″ in Dec. The photometry was calibrated on SAO stars (Tapia et al. 1986). Several 5-sec scans were taken at each wavelength at the position of the H-band peak. We computed flux densities relative to a scale of 1520, 980, 620, and 280 Jy at 1.25, 1.65, 2.2, and 3.8 μm respectively for a zero-mag star (Beckwith et al. 1976). We also mapped the 2.2 μm emission with a 7″ beam and a fast-mapping technique developed for the Wyoming Infrared Telescope (Hackwell et al. 1982), adapted to the 2.12 m telescope. The telescope was pointed at the 1.65 μm peak for the map center; the computer then moved the telescope to the first (SW) pixel, and did raster scans by stepping the wobbling secondary in Dec., while chopping. The measured intensity at each pixel was the difference between the on-source beam and a reference beam. After each Dec. scan, the telescope was offset in R.A. by one pixel. The map (Fig. 12) is 11 × 11 pixels, with 5″ grid spacing.

6.2. *Mass-to-near-IR light ratio*

How much mass is inside the radius of the nuclear ring? Wakamatsu & Nishida (1980) obtained a maximum Hα velocity gradient of 9.3 km s^{-1} arc s^{-1} at p.a. 121°±10°. They then assumed rigid-body rotation inside $R < 10''$, and adopted an inclination angle of 30°, to obtain a mass of 2 10^9 $M_\odot$ within this radius.

Similarly, the maximum CO velocity shift, $v_{CO} - v_{sys}$, where v_{sys} = systemic velocity, observed 9″ SE of the nucleus, is 70 km s^{-1}, so for the same inclination angle of 30°, the rotational velocity at a 9″ radius ($R = 450\, d_{10}$ pc) would be 140 km s^{-1}. If the spheroidal stellar bulge dominates the gravitational potential at $R < 450$ pc, the total mass $M(R)$ inside radius R would be $Rv^2(R)/G$, or 2.1 10^9 $M_\odot$, as in the estimate from Hα. Table 4 summarizes mass estimates for the circumnuclear components of NGC 4314; the H_2 mass is a large fraction of the dynamical mass.

We computed the 2.2 μm luminosity from $L(\theta) = 4\pi D^2 \nu S_\nu(\theta)$, where D = distance, ν = frequency, $S_\nu(\theta)$ = flux density in an aperture of diameter θ. From the observed 2.2 μm flux densities (Table 3), we get

$$L(5''.5, r = 140\,\text{pc}) = 1.3\ 10^8\, d_{10}^2\, L_\odot,$$
$$\text{and } L(14'', r = 350\,\text{pc}) = 3.8\ 10^8\, d_{10}^2\, L_\odot, \quad (3)$$

where L is the 2.2 μm luminosity of the region interior to the projected radius r, and $d_{10} = 1$ for a distance of 10 Mpc to NGC 4314. We did not correct the 2.2 μm flux density for extinction, since a visual extinction of 3 mag, for example, implies a 2.2 μm correction of only 8 mJy, the level of our measuring errors. Extrapolating to slightly larger radii and comparing with

© European Southern Observatory • Provided by the NASA Astrophysics Data System

1991A&A...244..257G

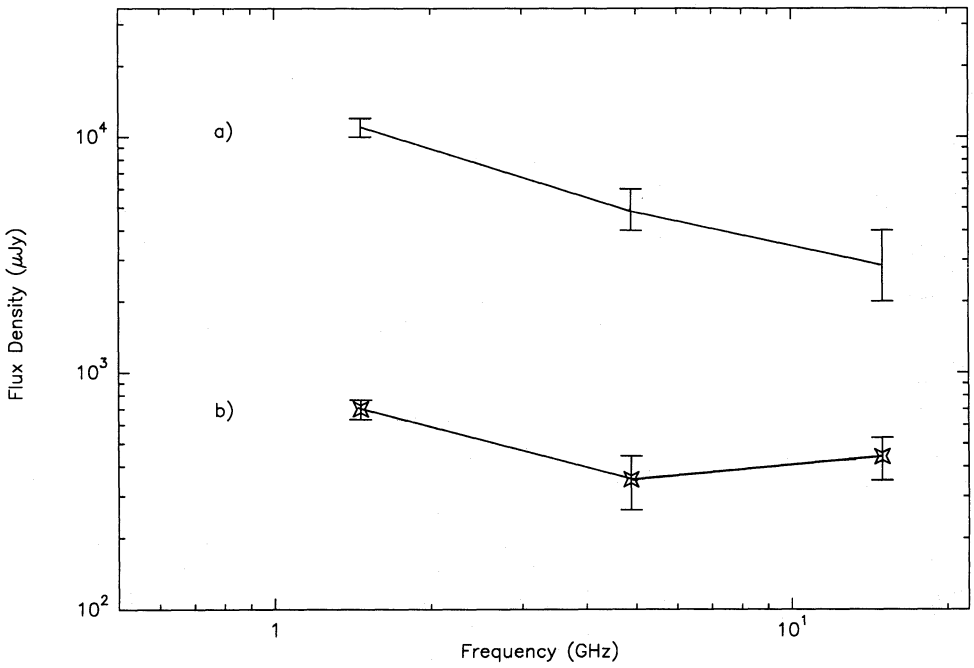

Fig. 8. Radio continuum spectra of the central region of NGC 4314. (a) Integrated flux. (b) Peak flux from the NW radio component at p.a. $\sim -25°$, as observed with 3.″5 beams

Table 4. Summary of derived quantities for the Nuclear ring of NGC 4314

Mass interior to $R = 450$ pc	
H II mass	$< 3\ 10^6\ M_\odot$
H I mass[a]	$4\ 10^6\ M_\odot$
H_2 mass	$2.5\ 10^8\ M_\odot$
Total mass	$2\ 10^9\ M_\odot$
Resonance model:	
Corotation radius	$72'' \simeq$ end of bar
Inner Lindblad resonance	$9'' \simeq$ nuclear ring
Angular velocity at ILR	$\Omega(450\,\mathrm{pc}) = 246\,\mathrm{km\,s^{-1}\,kpc^{-1}}$
Bar pattern speed	$\Omega_p = 36\,\mathrm{km\,s^{-1}\,kpc^{-1}}$
Epicyclic frequency at ring	$\kappa(450\,\mathrm{pc}) = 417\,\mathrm{km\,s^{-1}\,kpc^{-1}}$
Star formation in ring:	
FIR luminosity	$7\ 10^8\ L_\odot$
Lyman continuum photons	$2\ 10^{51}\ \mathrm{s^{-1}}$
Star formation rate	$0.06\ M_\odot\ \mathrm{yr^{-1}}$
Star formation rate/kpc^2	$0.12\ M_\odot\ \mathrm{yr^{-1}\,kpc^{-2}}$
Supernova rate in ring	$3\ 10^{-3}\ \mathrm{yr^{-1}}$

[a] The H I mass is the total for the whole galaxy. The data, however, are consistent with the H I being located at $R < 1.5$ kpc.

All quantities calculated for distance = 10 Mpc

the mass estimate from the Hα and CO velocities, we get a mass to 2.2 μm luminosity ratio of 3.1 $M_\odot/L_\odot$, not too different from the value of 2 $M_\odot/L_\odot$ in our galactic center (e.g. Sanders 1989), but rather different from the value of 0.08 to 0.3 $M_\odot/L_\odot$ for the central starburst zone in M 82 (estimated from Rieke et al. 1980).

7. Discussion

7.1. How does the gas get into the middle?

NGC 4314 seems to be a classic example of a galaxy with a strong bar whose gravitational torques drive gas in to a ring at the Inner Lindblad Resonance (e.g. Contopoulos 1980; Athanassoula 1984; Combes & Gerin 1985; Combes 1988). Numerical simulations suggest that the gravitational torque changes sign at the corotation radius, just beyond the ends of the bar. Gas outside the bar flows out to the Outer Lindblad Resonance; gas inside the corotation radius flows inward to the Inner Lindblad Resonance to form a nuclear ring (Combes 1988). The spiral dust lanes seen on optical images may be shock fronts where material piles up as it loses angular momentum to the bar (see e.g. Roberts et al. 1979). The torque acts on the matter in the arms of the inner, mini-spiral, forcing it inward to the ring. Once the gas is in the ring, it no longer feels the torque from the bar. If there are two Inner Lindblad Resonances, any nuclear gas should flow out to the circumnuclear ring. The CO maps and spectra of NGC 4314 suggest that gas indeed accumulates at the ring, and not at the nucleus, where the gravitational potential well is deepest.

Since we have no rotation curve from Hα, CO or H I, (the ionized gas and probably the molecular gas, is only in the nuclear ring), we modeled a mass distribution that would be consistent with our mass estimate at the nuclear ring, with an Inner Lindblad Resonance at the ring, and with corotation at the end of the bar. We modeled the galaxy by a bulge and disk (as we only deal with the circumnuclear and bar region, $R < 4$ kpc, we neglected the halo). The bulge was taken to be a Plummer (1911) sphere, with potential

$$\Phi(r) \propto \left(1 + \frac{r^2}{A_b^2}\right)^{-0.5} \tag{4}$$

and bulge scale $A_b = 400$ pc, while the disk was taken to be a Toomre (1963) disk, with surface density

$$\mu(r) = \int \varrho(r)\, dz \propto \left(1 + \frac{r^2}{A_d^2}\right)^{-1.5} \tag{5}$$

and disk scale $A_d = 1.6$ kpc. The projected radius r in the disk and height z above the plane are related to galactocentric radius R by $R^2 = r^2 + z^2$, and the disk/bulge mass ratio is $M_d/M_b = 6$. The model was adjusted to match the mass interior to 450 pc, derived

© European Southern Observatory • Provided by the NASA Astrophysics Data System

1991A&A...244..257G

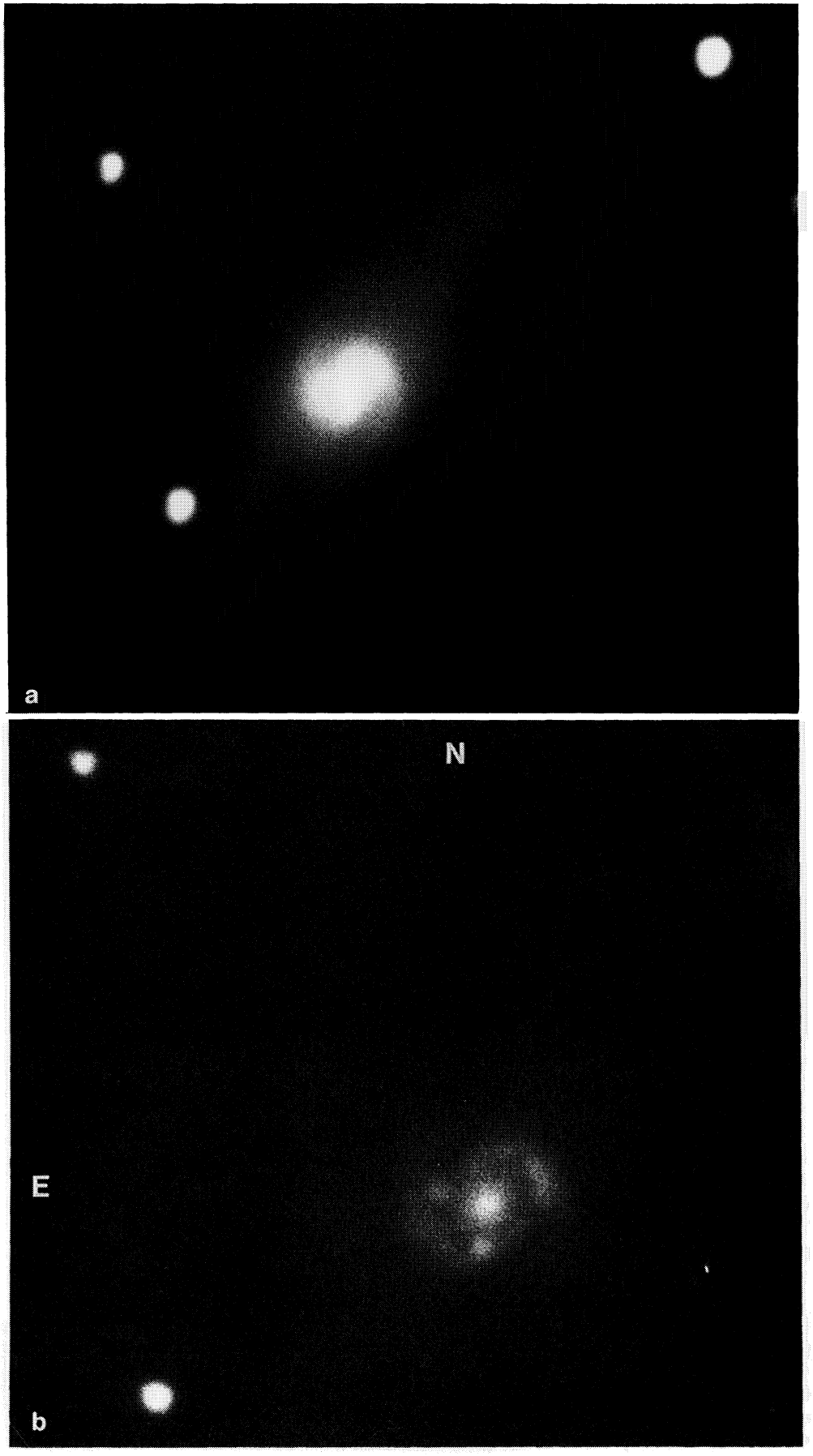

Fig. 9a and b. Optical photographs of NGC 4314 taken with the 2.12 m telescope at San Pedro, Mártir, Baja California, México, on Kodak 103aO emulsion: **a** 70 min exposure, north is up, east is left, **b** 12 min exposure. The two stars E and NE of the central region are separated by 75″

© European Southern Observatory • Provided by the NASA Astrophysics Data System

1991A&A...244..257G

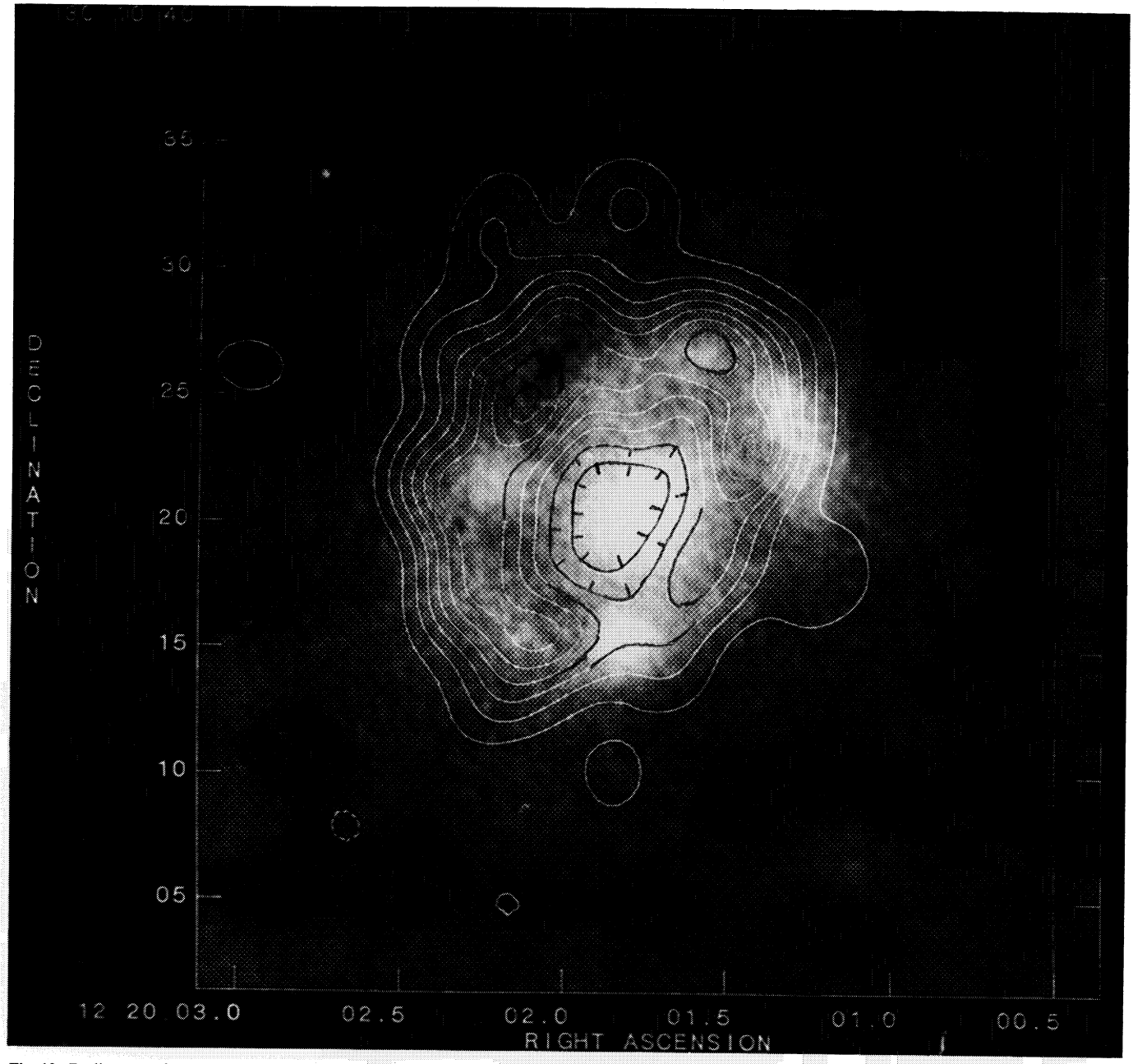

Fig. 10. Radio map of NGC 4314 at 20 cm superposed on the 12 min optical exposure. Radio contours are −0.14, +0.14, 0.24, 0.33, 0.42, 0.52, 0.61, 0.71, and 0.80 mJy beam^{-1}

from Hα and CO velocities corrected for inclination. The model is physically plausible but not unique.

In the model, the quantity $\Omega - \kappa/2$ is greatest at $R = 450$ pc, where $\Omega(R)$ is the angular velocity of the gas and stars, and $\kappa(R)$ is the epicyclic (radial oscillation) frequency:

$$\kappa^2 = 2\Omega\,(2\Omega + R\,d\Omega/dR) \qquad (6)$$

At this radius, the model predicts a rotational velocity of 111 km s^{-1}, an angular velocity $\Omega(9'') = 246\,d_{10}^{-1}$ km s^{-1} kpc^{-1}, and epicyclic frequency $\kappa(450\,\text{pc}) = 417$ km s^{-1} kpc^{-1}. For corotation at the ends of the bar ($R = 3.6$ kpc, 72″ from the nucleus), the model gives a pattern speed of the bar of $\Omega_p = 36\,d_{10}^{-1}$ km s^{-1} kpc^{-1}, which is consistent with the requirement $\Omega - \Omega_p = \kappa/2$ for Inner Lindblad Resonance(s) in the region 300 to 600 pc, that is, at the nuclear ring.

7.2. *Gas content of the nuclear ring*

How much gas is in the nuclear ring of NGC 4314? the CO luminosity gives 3 $10^8\,M_\odot$ in H_2, while the thermal radio flux gives $< 3\ 10^6\,M_\odot$ in H II. By contrast, our 21 cm observations give 4 $10^6\,M_\odot$ for H I interior to 1.5 kpc. Not only is most of the gas molecular, but the H_2 mass in the ring is also a significant fraction of the total mass within a radius of 450 pc of the nucleus, estimated to be 2 $10^9\,M_\odot$ from the CO and Hα velocities in this region. If the inner and outer radii of the ring are 4″ and 9″, then the area of the

© European Southern Observatory • Provided by the NASA Astrophysics Data System

1991A&A...244..257G

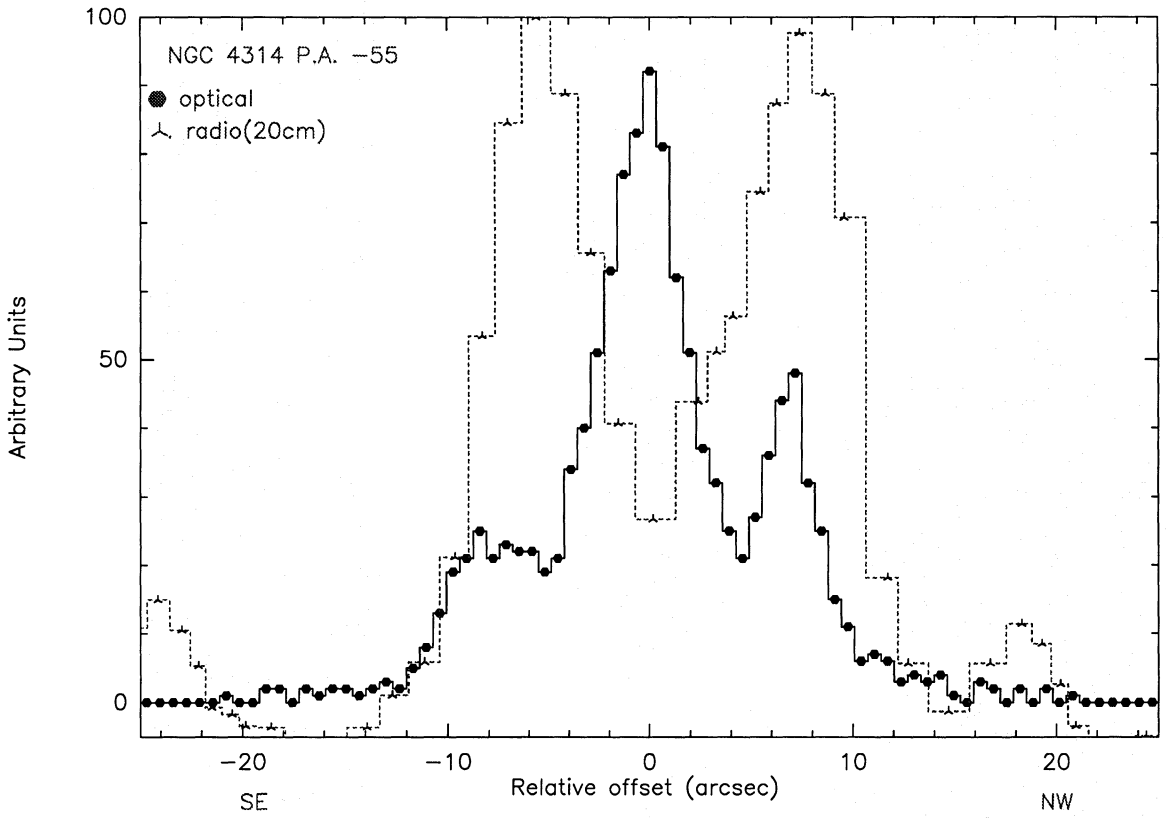

Fig. 11. Relative intensity of the radio and optical emission from the center of NGC 4314 at p.a. −55°. The plots show relative intensity at 20 cm (dotted line), and the digitized optical intensity (solid line)

ring is 5 $10^5 d_{10}^2$ pc^2, and the H_2 surface density is 500 $M_\odot$ pc^{-2}, independent of the galaxy's distance. If the ring thickness is 100 pc, the H_2 number density averaged over the whole ring is 100 cm^{-3}.

There are several arguments that the nuclear ring of NGC 4314 formed recently:

a) Very few nuclear rings have been detected in galaxies (Buta 1986), implying such rings have short lifetimes.

b) The molecular clouds must have been gathered in the nuclear ring of NGC 4314 on a relatively short time scale (10^7 to 10^8 yr?), as otherwise the O stars would have dispersed the gas.

c) The present level of star formation in the nuclear ring of NGC 4314 must be transitory; at the current star formation rate, the mass of stars accumulated in 5 Gyr would exceed the total dynamical mass of the nuclear region (Wakamatsu & Nishida 1980).

Of these arguments, *a)* may be affected by small plate scales and overexposure in surveys. Argument *b)* may not be true; the O stars may not be able to destroy the giant clouds. Argument *c)* holds for many galaxies, not just NGC 4314 (L_{FIR}/M_{H_2} is similar).

7.3. The gas in the nuclear ring makes stars

The concentration of so much molecular gas in such a small volume can certainly explain the presence of H II regions and supernovae in the ring. The existence of massive stars in the nuclear ring of NGC 4314 is consistent with the IRAS (1985) flux densities of 0.25, 0.39, 3.7, and 7.3 Jy at 12, 25, 60, and 100 μm respectively. If the flux density varies as frequency times the black body curve, then the dust temperature is 35 K, as in galaxies with bursts of star formation. Also, the far infrared colors of NGC 4314 and the 20 cm/FIR flux ratio are similar to those in starburst galaxies (Helou et al. 1985; Helou 1986; note, however, the different radio and FIR beams).

From the formulae in Helou et al. (1985), the far-infrared flux is 2.1 10^{-13} W m^{-2}, and the FIR luminosity is 7 $10^8 d_{10}^2 L_\odot$. This FIR luminosity corresponds to a star formation rate of 8 $10^{-11} L_{tot} M_\odot$ yr^{-1}, or $0.06 d_{10}^2 M_\odot$ yr^{-1}. A similar rate is obtained from the Hα luminosity of $10^5 L_\odot$ from the central region of this galaxy (Wakamatsu & Nishida 1980; see formula by Pogge & Eskridge 1987). Furthermore, if supernova remnants are the main sources of the non-thermal radio emission, then the observed flux corresponds to 0.003 supernovae per year in the central region (see formulae by Ulvestad 1982), which is also consistent with the star formation rate estimated above. Table 4 summarizes the derived parameters for the nuclear ring of NGC 4314.

Is it a "starburst", in rate, efficiency, or short duration? The star formation rate in NGC 4314 is about the same as in Virgo cluster spirals, although it evidently applies only to the nuclear ring of NGC 4314, and not the whole galaxy, as in the Virgo spirals surveyed by Scoville et al. (1983). If we normalize by the surface area of the ring, the star formation rate is 0.12 $M_\odot$ yr^{-1} kpc^{-2}, about the same as between $R = 4$ and 6 kpc in our Galaxy, where the Milky Way star formation rate has a very steep peak (cf. Güsten and Mezger 1983). However, with an available H_2 mass of 3 $10^8 M_\odot$ in the ring of NGC 4314, its current star formation rate of $0.06 d_{10}^2 M_\odot$ yr^{-1} can be sustained for 5 Gyr.

Therefore, although star formation is greatly enhanced in the nuclear ring relative to the outer arms, there is enough molecular

© European Southern Observatory • Provided by the NASA Astrophysics Data System

1991A&A...244..257G

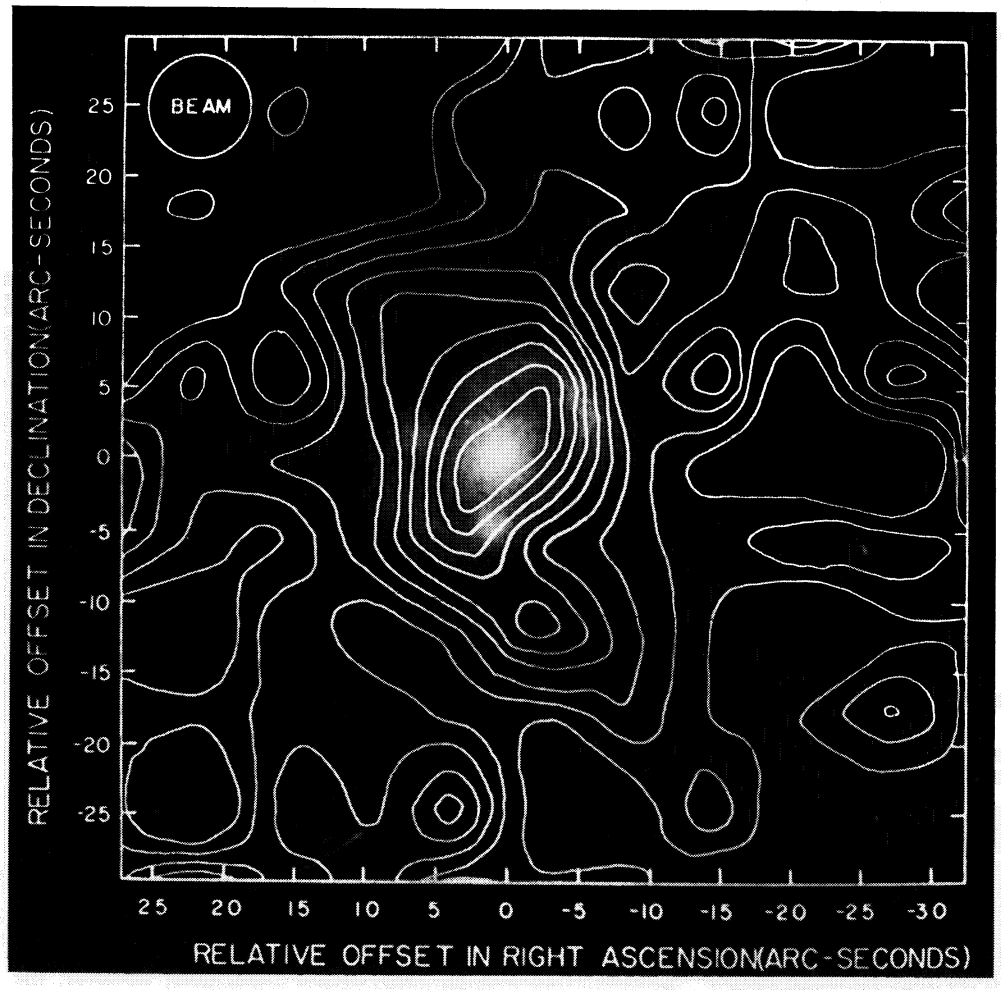

Fig. 12. Isophotes of 2.2 μm emission, observed with a 7″ aperture, superposed on an optical image of the central region of NGC 4314. The optical image was taken on Kodak 103Oa emulsion with no filters. R.A., Dec. offsets are relative to $(0,0) = 12^h20^m01^s.8$, 30°10′20″ (±1″) (1950). Contours: 1 to 9 in steps of 1; unit = 4.2 mJy beam^{-1}

gas in the ring to ensure a steady rate of star formation for a long time. Hence it is not the nuclear ring that is unusual, but rather the outer spiral arms – unlike the normal spiral arms of other galaxies, the outer arms of NGC 4314 have no gas, no H II regions, no radio continuum, and possibly no star formation at all.

7.4. What happened to the H I?

The most spectacular result of this study is the extreme H I deficiency in NGC 4314, not only in the inner region, but also in the outer parts of the galaxy. It may be that gas in the outer region was stripped away in a previous collision of NGC 4314 with another member of the NGC 4276 group, which contains at least 13 galaxies within a radius of 500 kpc (de Vaucouleurs 1975). In a fast collision, the H I gas can be evaporated from a galaxy very rapidly, while the H_2 gas can remain within the galaxy because of its smaller filling factor (Valluri & Jog 1990, see also Kenney & Young 1989). As NGC 4314 is a very symmetric galaxy, without tidal tails, any interaction with another galaxy probably occurred in the distant past (> 1 Gyr). If such a collision did indeed get rid of the H I, leaving the H_2, then the lifetime of the molecular clouds must also be long, since no new reservoir of H I has formed from dissociating H_2.

The very unusual nature of NGC 4314 merits further study. In particular, it would be worth making hydrodynamic simulations of the sequence: ancient galaxy collision – evaporation of H I – formation of a bar – sweeping of the remaining (molecular) gas into a nuclear ring – era of star formation –, in order to see if a plausible explanation can be found for the remarkable H_2/H I ratio in this galaxy.

8. Conclusions

Our Arecibo observations show NGC 4314 to be highly deficient in H I, while our CO observations show abundant molecular gas near the center of the galaxy. The VLA observations of the radio continuum, as well as the optical images show that the concentration of molecular gas has produced massive stars ionizing H II regions in a circumnuclear ring of radius 6″ (inner radius 4″, outer radius 9″). Explosions of these massive stars presumably generate the relativistic particles emitting nonthermal radio radiation in the ring. Our infrared observations allow us to estimate the mass-to-2 μm light ratio interior to the ring. Specific conclusions are:

1) The CO is concentrated in within a radius of 500 pc of the nucleus, probably in the nuclear ring; in this region, the H_2 mass is 2.5 10^8 $M_\odot$. The CO $I(2-1)/I(1-0)$ ratio is 0.7, characteristic of subthermal excitation, and the $^{12}CO/^{13}CO$ ratio is 6 to 12.

2) The total H I mass is 4 10^6 $M_\odot$, a surprisingly low value. *The ratio of H_2 to H I mass is ≧60-to-1!* No H I has been detected outside $R = 30''$ (1.5 kpc). The entire galaxy is deficient in H I, not just the central part.

© European Southern Observatory • Provided by the NASA Astrophysics Data System

1991A&A...244..257G

3) Radio continuum emission is only detected from the nuclear ring; its distribution is similar to the visible light in the ring.

4) No radio continuum is detected from the optical nucleus, to a limit of 0.1 mJy at 20 cm.

5) No radio continuum emission is detected from the stellar bar ($R > 15''$), or the outer spiral arms, to a level of 0.16 mJy in the low-resolution maps at 20 and 6 cm.

6) No polarized radio emission was detected, to 15% r.m.s. of the 6 and 20 cm peaks.

7) The radio continuum emission may be completely non-thermal, with a spectral index of -0.4, but is more likely to be a mix of thermal and synchrotron radiation. The thermal flux is $< 50\%$ at 20 cm, but may be 85% at 2 cm.

8) From the estimated thermal flux at 2 cm, the electron density of the H II regions is $> 25\,\mathrm{cm}^{-3}$. The Lyman continuum photon rate in each radio peak is equivalent to a few hundred O7 stars.

9) The stellar mass inside of $R = 450$ pc predicted from the CO velocities is $2\ 10^9\ M_\odot$.

10) From a mass model of the galaxy which reproduces the observed velocities, the pattern speed of the bar is $\Omega_p = 36\, d_{10}^{-1}\ \mathrm{km\,s^{-1}\,kpc^{-1}}$, and at the ring, the angular speed and epicyclic frequencies are 246 and 417 $\mathrm{km\,s^{-1}\,kpc^{-1}}$, respectively, consistent with an Inner Lindblad Resonance at the molecular ring.

11) From the FIR luminosity, the star formation rate is estimated to be $0.06\ M_\odot\ \mathrm{yr}^{-1}$. From the non-thermal radio flux, the supernova rate is the nuclear ring is $0.003\ \mathrm{yr}^{-1}$. The molecular gas in the ring is sufficient to sustain this rate of star formation for 5 Gyr. Hence the activity need not be a transitory "starburst".

12) The extreme value of the $H_2/H\,I$ ratio in this galaxy might be the result of a collision with another galaxy at an epoch much earlier than the formation of the nuclear ring.

Acknowledgements. We thank the staffs of the IRAM 30 m and Arecibo telescopes, the VLA, and the 2.12 m telescope in San Pedro Martir, México, for help with observing, and M.A. García-Zárate for photographic work and preparation of figures. The staff at CICESE (Ensenada, Mexico) kindly made available their PDS. J.A.G.-B. was supported by CONACYT (Mexico) grants PCCBCNA-722419, 723437 and PCCBBNA-022688, grants from the American Astronomical Society and from Aeromexico, and fellowships from the Alexander von Humboldt Foundation and from the Max Planck Gesellschaft, West Germany. The Arecibo telescope of the National Astronomy and Ionosphere Center is operated by Cornell University under contract with the U.S. National Science Foundation. The National Radio Astronomy Observatory is operated by Associated Universities under contract with the U.S. National Science Foundation.

References

Athanassoula E., 1984, Phys. Rep. 114, 319
Beckwidth S., Evans N.J., Becklin E.E., Neugebauer G., 1976, ApJ 208, 390
Benedict G.F., 1980, AJ 85, 513
Bridle A.H., Davis M.M., Fomalont E.B., Lequeux J., 1972, AJ 77, 405
Burbidge E.M., Burbidge G.R., 1962, ApJ 135, 694
Buta R., 1986, ApJS 61, 609
Clark B.G., 1980, A&A 89, 377
Combes F., Gerin M., 1985, A&A 150, 327
Combes F., 1988, in: Galactic and Extragalactic Star Formation, eds. R.E. Pudritz, M. Fich, Kluwer, Dordrecht, p. 475
Contopoulos G., 1980, A&A 81, 198
de Vaucouleurs G., 1975, in: Galaxies and the Universe, eds. A. Sandage, M. Sandage, J. Kristian, Univ. Chicago Press, p. 557
de Vaucouleurs G., 1979, ApJ 227, 729
Devereux N., Becklin E.E., Scoville N., 1987, ApJ 312, 529
Duric N., 1986, ApJ 304, 96
Duric N., Seaquist E.R., Crane P., Davis L.E., 1986, ApJ 304, 82
Gallagher J.S., Faber S.M., Balick B., 1975, ApJ 202, 7
Gioia I.M., Fabbiano G., 1987, ApJS 63, 771
Güsten R., Mezger P.G., 1983, Vistas Astron. 26, 159
Hackwell J.A., Gradalen G.L., Gehrz R.D., 1982, ApJ 252, 250
Haynes M.P., Giovanelli R., 1984, ApJ 89, 758
Haynes M.P., Giovanelli R., Chincarini G.L., 1984, ARA&A 22, 445
Helou G., Soifer B.T., Rowan-Robinson M., 1985, ApJ 298, L7
Helou G., 1986, ApJ 311, L33
Huchra J.P., Geller M.J., 1982, ApJ 257, 423
Huchtmeier W.K., 1982, A&A 110, 121
Hummel E., 1980, A&AS 41, 151
Hummel E., van der Hulst J.M., Dickey J.M., 1984, A&A 134, 207
Hummel E., van der Hulst J.M., Keel W.C., 1987, A&A 172, 32
Humason M.L., Mayall N.U., Sandage A.R., 1956, AJ 61, 97
IRAS Point Source Catalog, 1985, U.S. Govt. Printing Office, Washington, D.C.
Kenney J.D.P., Young J.S., 1989, ApJ 344, 171
Kenney J.D.P., Young J.S., Hasegawa T., Nakai N., 1990, ApJ 353, 460
Krumm N., Salpeter E.E., 1976, BAAS 8, 395
Kelton P.W., 1980, AJ 85, 89
Lequeux J., 1980, in: Star Formation, eds A. Maeder, L. Martinet, Geneva Observatory, p. 75
Lynds B.T., Furenlid I., Rubin J., 1973, ApJ 182, 659
Lynds B.T., 1974, ApJS 28, 391
Mezger P., Henderson A.P., 1967, ApJ 147, 471
Morgan W.W., 1958, PASP 70, 364
Ondrechen M.P., 1985, AJ 90, 1474
Plummer H.C., 1911, MNRAS 71, 460
Pogge R.W., 1989, ApJS 71, 433
Pogge R.W., Eskridge P.B., 1987, AJ 93, 291
Rengarajan T.N., Verma R.P., 1986, A&A 165, 300
Rieke G.H., Lebofsky M.J., Thompson R.I., Low F.J., Tokunaga A.T., 1980, ApJ 238, 24
Roberts W.W., Huntley J.M., van Albada G.D., 1979, ApJ 233, 67
Roth M., Iriarte A., Tapia H., Reséndiz G., 1984, Rev. Mex. Astron. Astrofis. 9, 25
Sandage A., 1961, The Hubble Atlas of Galaxies, Carnegie Institution, Washington D.C.
Sandage A., Tammann G.A., 1975, ApJ 196, 313
Sanders R.H., 1989, in: The Center of the Galaxy, IAU Symp. 136, ed. M. Morris, Kluwer, Dordrecht, p. 77
Scoville N.Z., Becklin E.E., Young J.S., Capps R.W., 1983, ApJ 271, 512
Solomon P., Sage L., 1988, ApJ 334, 613
Tapia M., Neri L., Roth M., 1986, Rev. Mex. Astron. Astrofis. 13, 115
Thompson A.R., Clark B.G., Wade C.M., Napier P.J., 1980, ApJS 44, 151
Toomre A., 1963, ApJ 138, 385
Tully R.B., 1987, ApJ 321, 280

© European Southern Observatory • Provided by the NASA Astrophysics Data System

1991A&A...244..257G

Tully R.B., 1988, Nearby Galaxies Catalog, Cambridge Univ. Press, Cambridge, p. 103, p. 189
Turner E.L., Gott J.R., 1976, ApJS 32, 409
Ulvestad J.S., 1982, ApJ 259, 96
Valluri M., Jog C.J., 1990, ApJ 357, 367
van den Bergh S., 1976, ApJ 206, 883
Vorontsov-Vel'yaminov B.A., Zaitseva G.V., Lyutyi V.M., 1972, AZh 49, 93; SvA 16, 71
Wakamatsu K., Nishida M.T., 1980, PASJ 32, 389
Wray J.D., 1988, The Color Atlas of Galaxies, Cambridge Univ. Press, Cambridge, Plate 56
Young J.S., Knezek P.M., 1989, ApJ 347, L55

© European Southern Observatory • Provided by the NASA Astrophysics Data System